2016

Structure, magnetism, and electron-transport properties of Mn_2CrGa-based nanomaterials

Wenyong Zhang
University of Nebraska-Lincoln, wenyong.zhang@unl.edu

Parashu Kharel
University of Nebraska-Lincoln, pkharel2@unl.edu

Ralph Skomski
University of Nebraska-Lincoln, rskomski2@unl.edu

Shah R. Valloppilly
University of Nebraska-Lincoln, svalloppilly2@unl.edu

XINGZHONG LI
Nebraska Center for Materials and Nanoscience, xli2@unl.edu

See next page for additional authors

Structure, magnetism, and electron-transport properties of Mn_2CrGa-based nanomaterials

Wenyong Zhang,[1,2] Parashu Kharel,[1,3] Ralph Skomski,[1,2] Shah Valloppilly,[1] Xingzhong Li,[1] and David J. Sellmyer[1,2]
[1]*Nebraska Center for Materials and Nanoscience, University of Nebraska, Lincoln, NE 68588 USA*
[2]*Department of Physics and Astronomy, University of Nebraska, Lincoln, NE 68588 USA*
[3]*Department of Physics, South Dakota State University, Brookings, SD 57007 USA*

(Presented 12 January 2016; received 3 November 2015; accepted 14 January 2016; published online 11 March 2016)

Mn_2CrGa in the disordered cubic structure has been synthesized using rapid quenching and subsequent annealing. The cubic phase transforms to a stable tetragonal phase when a fraction of Cr or Ga is replaced by Pt or Al, respectively. All samples are ferrimagnetic with high Curie temperatures (T_c); Mn_2CrGa exhibits the highest T_c of about 813 K. The tetragonal samples have appreciable values of magnetocrystalline anisotropy energy, which leads to an increase in coercivity (H_c) that approaches about 10 kOe in the Pt-doped sample. The H_c linearly increases with a decrease of temperature, concomitant with the anisotropy change with temperature. All samples are metallic and show negative magnetoresistance with room-temperature resistivities on the order of 1 mΩcm. The magnetic properties including high T_c and low magnetic moment suggest that these tetragonal materials have potential for spin-transfer-torque-based devices. [http://dx.doi.org/10.1063/1.4944403]

INTRODUCTION

Heusler compounds have attracted much recent attention because of their multiple interesting and tunable properties with prospects for spintronic applications.[1,2] Heusler compounds include a wide range of interesting materials such as half-metallic ferro-, ferri-, or antiferromagnets, high perpendicular-magnetic-anisotropy materials, shape-memory alloys, spin-gapless semiconductors, skyrmions, topological insulators, and magnetocalorics.[3–8] Heusler alloys with high spin polarization at the Fermi level, high perpendicular magnetic anisotropy, low magnetization and a Curie temperature much above room temperature have been extensively investigated as prospective materials for novel devices which employ spin-transfer torque (STT) phenomena such as STT magnetic random access memories.[9,10] Materials having these properties are expected to minimize the switching time and switching current while maintaining thermal stability, leading to a fast and energy-efficient STT device. One of the Heusler materials with these characteristics is tetragonal $Mn_{3-x}Ga$, which is synthesized by high-temperature solid-phase transformation.[11] However, it is difficult to obtain high-quality single-phase films with desired perpendicular magnetic anisotropy with this synthesis process. The other two drawbacks of $Mn_{3-x}Ga$ for STT application are relatively high saturation magnetization and large lattice mismatch with MgO. Low saturation magnetization is desired to maintain a balance between switching current, speed of switching and thermal stability whereas a lattice mismatch with MgO substantially reduces the tunnel magnetoresistance (TMR) in devices.[12] Therefore, it is essential to investigate additional new materials with low magnetization, high Curie temperature and high perpendicular anisotropy. Our interest is to investigate a Mn-based Heusler compound Mn_2CrGa which has been predicted to be a half-metallic ferromagnet with high Curie temperature in the cubic structure, while in the tetragonal structure it shows a large magnetocrystalline anisotropy of about 24.6 Mergs/cm^3.[13,14] Further, since the magnetic properties

of Heusler compounds can be tuned by adjusting the compositions, we also study the effect of a small amount of Pt substitution for Cr, and Al substitution for Ga on the structural and magnetic properties of Mn_2CrGa. Since Mn_2PtGa crystallizes in the tetragonal structure, it is expected that the Pt substitution for Cr might help to stabilize the tetragonal structure of Mn_2CrGa whereas the Al substitution for Ga may lead to structural distortion due to its relatively small atomic radius resulting in non-cubic structure.[15,16] Here, we report our experimental investigation of the structural, microstructural, magnetic and electron-transport properties of cubic Mn_2CrGa, and tetragonal $Mn_2CrGa_{0.8}Al_{0.2}$ and $Mn_2Cr_{0.75}Pt_{0.25}Ga$ alloys prepared by arc-melting, rapid quenching and annealing.

EXPERIMENTAL METHODS

The Mn_2CrGa, $Mn_2Cr_{0.75}Pt_{0.25}Ga$, and $Mn_2CrGa_{0.8}Al_{0.2}$ ingots were prepared by arc melting high-purity constituent elements (99.95%) in an argon atmosphere. An extra 3% of Mn by weight was used to compensate the weight loss during arc melting. Rapid quenching in a melt-spinner chamber was used to obtain these alloys in the form of ribbons. During rapid quenching, the speed of the rotating copper wheel was maintained at 20 m/s to obtain crystalline ribbons. These ribbons are about 2 mm wide and 50 μm thick. In order to obtain the equilibrium crystal structure, the ribbon samples were annealed at 500 ^oC for 2 hours in a tubular furnace pumped to a base pressure of about 10^{-7} Torr. The crystal structure and phase components of the samples were examined using a Rigaku D/Max-B x-ray diffractometer (XRD) with Co K_α radiation. A Rietveld analysis of the x-ray diffraction patterns was done using TOPAS software. The microstructure of the ribbons including elemental mapping was studied using a FEI Tecnai Osiris Transmission Electron Microscope (TEM). The isothermal magnetic hysteresis loops $M(H)$ and thermomagnetic curves $M(T)$ were measured using a vibrating-sample magnetometer in a Quantum Design physical property measurement system (PPMS). Electron transport properties were measured by the four-point-probe method using the PPMS.

RESULTS AND DISCUSSION

Figure 1 shows the room-temperature powder XRD patterns of the Mn_2CrGa, $Mn_2Cr_{0.75}Pt_{0.25}Ga$, and $Mn_2CrGa_{0.8}Al_{0.2}$ ribbons. As shown in Fig. 1(a), all diffraction peaks in the XRD pattern of Mn_2CrGa ribbons are indexed with the standard pattern simulated for its cubic structure. The Rietveld analysis of the patterns suggests that the samples have B2-type disordered cubic structure with lattice constant a = 5.93 Å, which is slightly larger than the value (5.77 Å) predicted for its ordered $L2_1$ structure.[14] As shown in Figs. 1(b) and 1(c), most of the intense diffraction peaks in the XRD patterns of $Mn_2Cr_{0.75}Pt_{0.25}Ga$ and $Mn_2CrGa_{0.8}Al_{0.2}$ are indexed with the patterns simulated for tetragonal structure. Although the Pt and Al substitution helped to stabilize the tetragonal structure, the resulting samples were not completely free from secondary phases. It was found that $Mn_2Cr_{0.75}Pt_{0.25}Ga$ and $Mn_2CrGa_{0.8}Al_{0.2}$ ribbons contain respectively about 10 wt% of rhombohedral CrGa and 13 wt% of cubic $(Mn,Cr)_3Al$ as secondary phases. The diffraction peaks of the Pt and Al substituted samples are wider than that of the undoped samples indicating that the substituted elements caused a reduction in grain size.

The phase components in the samples were determined with the help of STEM imaging with elemental mapping. Figure 2 shows the high-angle annular dark field (HAADF) and element-mapping images of the $Mn_2Cr_{0.75}Pt_{0.25}Ga$ and $Mn_2CrGa_{0.8}Al_{0.2}$ ribbons. As shown in Fig. 2(a), the white and gray areas in the HAADF image corresponds to the tetragonal $Mn_2Cr(Ga, Al)$ matrix phase and cubic $(Mn, Cr)_3Al$ phase, respectively. In the HAADF image, the image contrast is related to the average atomic number of the compound, where the areas with higher contrast have larger average atomic number. The needle-like areas in the HAADF image of Figure 2(b) are from rhombohedral CrGa, which has relatively small atomic number and thus looks dark. The matrix tetragonal $Mn_2(Cr,Pt)Ga$ phase has large atomic number and thus looks bright. The elemental mapping shows that the matrix phase is Pt-rich, corresponding to the $Mn_2(Cr,Pt)Ga$ phase, and the

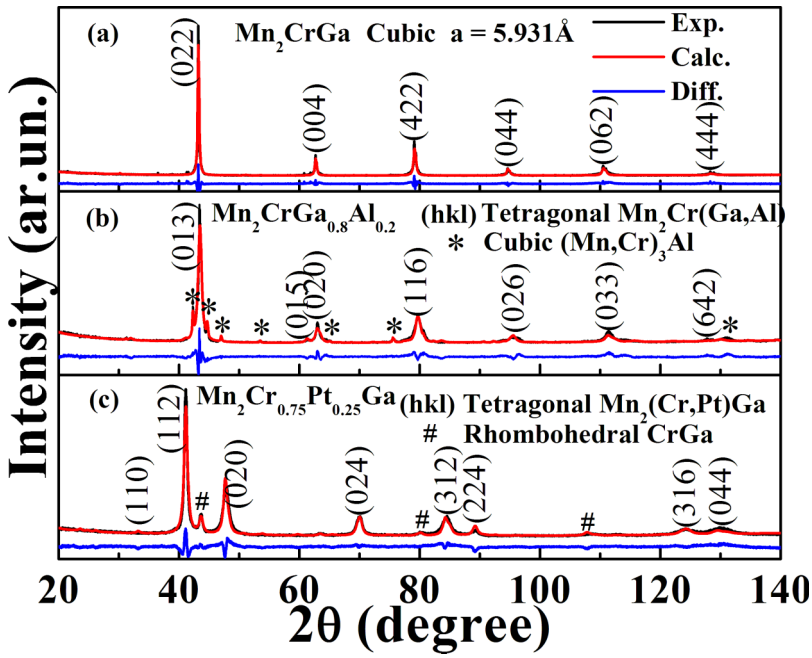

FIG. 1. XRD patterns of the Mn_2CrGa (a), Ptdoped (b), Al-doped (c) ribbon powders.

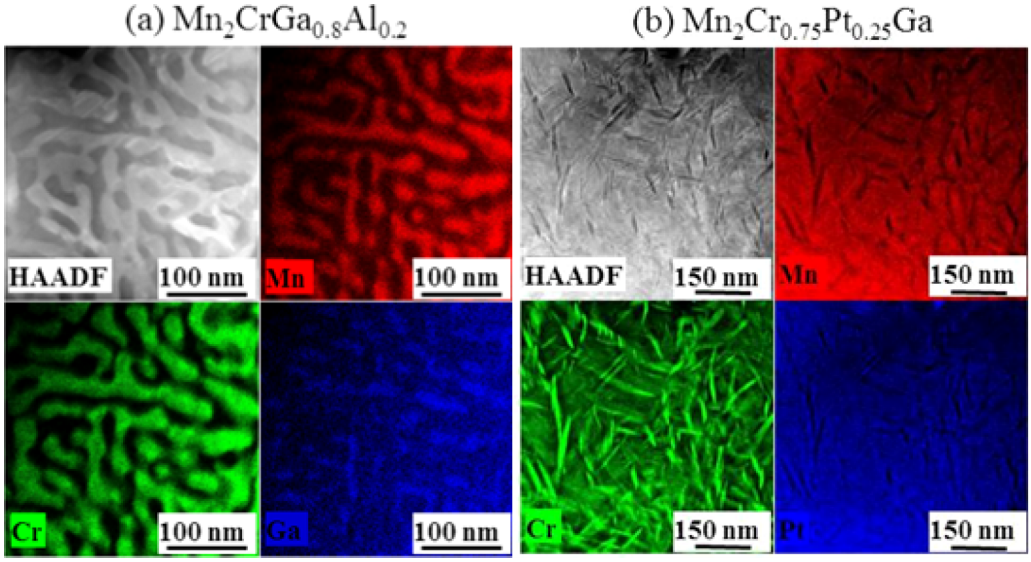

FIG. 2. HAADF and element-mapping images of the Al- and Pt-doped specimens prepared from corresponding ribbons.

needle-like phase is Cr-rich, corresponding to the CrGa phase. These observations are consistent with the XRD data as discussed above.

The thermomagnetic curves $M(T)$ of the ribbon samples measured at 1 kOe between 300 K and 900 K are shown in Fig. 3. The $M(T)$ curves are smooth and have single magnetic transitions corresponding to the Curie temperature (T_C). All samples exhibit high Curie temperatures, much above room temperature. The undoped Mn_2CrGa exhibits a highest T_c of 813 K where the T_c decreases with Pt and Al substitution leading to the lower values of 789 K and 645 K for $Mn_2CrGa_{0.8}Al_{0.2}$ and $Mn_2Cr_{0.75}Pt_{0.25}Ga$, respectively.

Figure 4(a) shows the room-temperature magnetic hysteresis curves of the Mn_2CrGa, $Mn_2CrGa_{0.8}Al_{0.2}$, and $Mn_2Cr_{0.75}Pt_{0.25}Ga$ ribbons. The $M(H)$ loops of all three samples are not

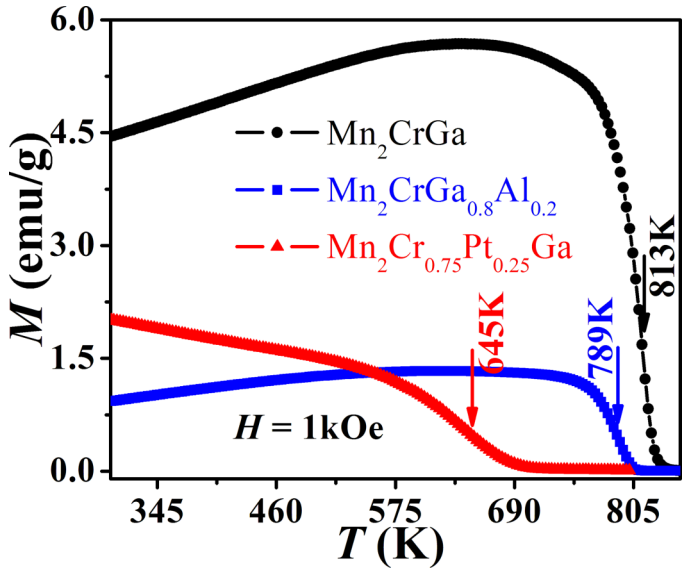

FIG. 3. $M(T)$ curves of the Mn_2CrGa, $Mn_2Cr_{0.75}Pt_{0.25}Ga$, and $Mn_2CrGa_{0.8}Al_{0.2}$ ribbons.

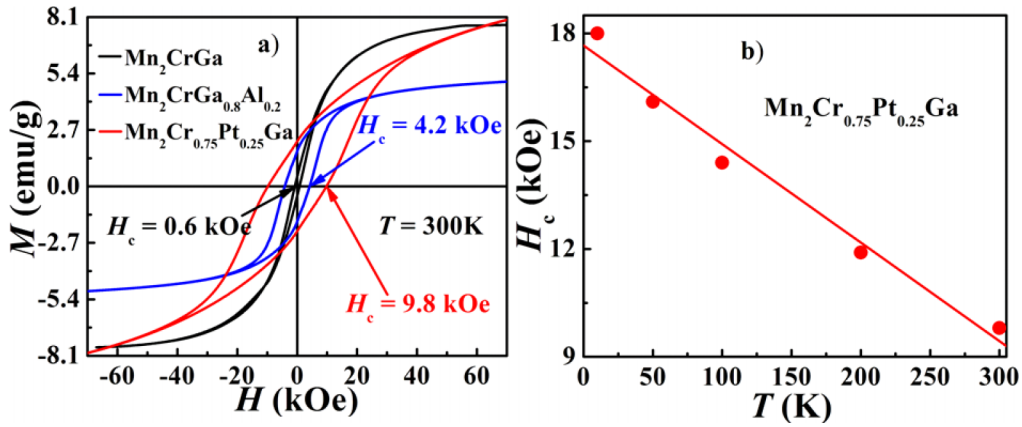

FIG. 4. (a) $M(H)$ curves of the Mn_2CrGa, $Mn_2CrGa_{0.8}Al_{0.2}$, and $Mn_2Cr_{0.75}Pt_{0.25}Ga$ ribbons, (b) temperature dependence of H_c.

completely saturated even at 70 kOe indicating that they have high magnetic anisotropy. The high-field magnetization of the cubic Mn_2CrGa is 7.7 emu/g (0.4 μ_B/f.u.) which is smaller than the value (1 μ_B/f.u.) predicted by the Slater-Pauling rule for its half-metallic ferromagnetic phase. The high-field magnetization is nearly stable against Pt doping (8 emu/g) but shows a substantial decrease (5 emu/g) with Al substitution for Ga. This reduction of M at 70 kOe may arise from disorder-induced antiferromagnetic ordering or a reduction of the moment due to the tetragonal distortion.[17] The Mn_2CrGa sample shows soft magnetic behavior with a small coercivity of about 0.6 kOe at room-temperature. There is a substantial increase in the coercivity due to Al and Pt doping where the coercivities of $Mn_2CrGa_{0.8}Al_{0.2}$, and $Mn_2Cr_{0.75}Pt_{0.25}Ga$ ribbons are 4.2 kOe and 9.8 kOe respectively. The large values of coercivities in these samples are caused by the existence of magnetocrystalline anisotropy due to the tetragonal structure of these alloys or the shape anisotropy of the magnetic phase. The room-temperature magnetocrystalline anisotropy constant for the Pt-doped sample was estimated to be 5.0 Mergs/cm^3 using the law of approach-to-saturation. Further, as shown in Fig 4(b), the coercivity of the Pt-doped sample linearly decreases from 18.0 kOe at 10 K to 9.8 kOe at 300 K, which is attributed to the decrease in the magnetocrystalline anisotropy constant with the increase in temperature.

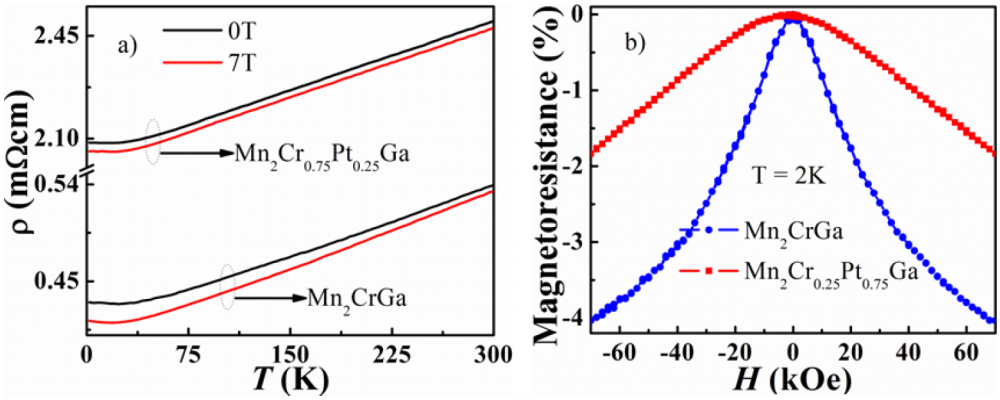

FIG. 5. (a) Temperature dependence of resistivity for the Mn_2CrGa and $Mn_2Cr_{0.75}Pt_{0.25}Ga$ and (b) magnetoresistance vs H at 2K.

Figure 5(a) shows the temperature dependence of resistivity ρ(T) for the Mn_2CrGa and $Mn_2Cr_{0.75}Pt_{0.25}Ga$ ribbons measured at H = 0 kOe and 70 kOe and Fig. 5(b) shows the magnetoresistance $(\rho_H-\rho_0)/\rho_0$ as function of magnetic field measured at 2 K. Both ribbons show poor metallic conductivity with their room-temperature resistivities being on the order of 1 mΩcm. The resistivities of the ribbons decrease almost linearly with decreasing temperature and pass through a minimum at 26K. The resistivity of the Pt-doped ribbon is slightly larger than that of the undoped ribbon. The values of the residual resistivity ratio (RRR) defined as ρ_{300K}/ρ_{2K} for the two ribbons are slightly larger than one. These small values of RRR may indicate that there is significant scattering of conduction electrons at the defect centers of the disordered samples leading to the low-temperature resistivity minima at 26 K. The resistivities of both Mn_2CrGa and $Mn_2Cr_{0.75}Pt_{0.25}Ga$ ribbons decrease (negative magnetoresistance) when measured at 70 kOe consistent with the suppression of electron scattering from moments being aligned due to the high magnetic field. As shown in Fig. 5(b), the MR of the undoped ribbon increases with increasing magnetic field, with a tendency towards saturation. In contrast, the MR of the Pt-doped ribbon shows a nearly linear variation with field at $H \geq 20$ kOe.

CONCLUSIONS

We have synthesized cubic Mn_2CrGa with B2-type disorder but the crystal structure transforms to tetragonal when Cr is partially substituted by Pt or Ga is partially replaced by Al. Both the doped samples contain a small amount of non-magnetic secondary phases. All three samples show ferro- or ferrimagnetic spin order with the Curie temperature much above room temperature. These tetragonal samples have low high-field magnetization (8 emu/g) and high coercivity (4.2 kOe for the $Mn_2CrGa_{0.8}Al_{0.2}$ and 9.8 kOe for the $Mn_2Cr_{0.75}Pt_{0.25}Ga$). The high value of coercivity in Pt-doped ribbon is likely caused by the combined effect of high magnetic anisotropy and presence of pinning centers from a needle-shaped secondary phase. All the ribbons show metallic conductivity and negative magnetoresistance with room temperature resistivities of 0.54 mΩcm for the Mn_2CrGa and 2.5 mΩcm for the $Mn_2Cr_{0.75}Pt_{0.25}Ga$. These observed values of low magnetization, high anisotropy, high Curie temperature and moderate conductivity are desired for STT applications. Further work is necessary to understand the magnetic and transport properties of these interesting Heusler-type substitutional alloys.

ACKNOWLEDGEMENT

This work supported by NSF-DMREF: SusChEM (Award Number: 1436385). Research was performed in part in Facilities of the Nebraska Center for Materials and Nanoscience, which is

supported by the National Science Foundation under Award NNCI: 1542182, and the Nebraska Research Initiative. The authors would like to thank Dr. Arti Kashyap for the helpful discussions.

[1] F. Casper, T. Graf, S. Chadov, B. Balke, and C. Felser, Semicond. Sci. Techn. **27**, 063001 (2012).
[2] T. Graf, C. Felser, and S.S.P. Parkin, Prog. Sol. Stat. Chem. **39**, 1 (2011).
[3] C. Felser, G.H. Fecher, and B. Balke, Angew. Chem. **119**, 680 (2007).
[4] P. Kharel, W.Y. Zhang, R. Skomski, S. Valloppilly, Y. Huh, R. Fuglsby, S. Gilbert, and D.J. Sellmyer, J. Phys. D: Appl. Phys. **48**, 245002 (2015).
[5] S. Ouardi, G.H. Fecher, and C. Felser, Phys. Rev. Lett. **110**, 100401 (2013).
[6] M. Franz, Nature Materials **9**, 536 (2010).
[7] X. Yan, G. Joshi, W.S. Liu, Y.C. Lan, H. Wang, S.Y. Lee, J. W. Simonson, S.J. Poon, T.M. Tritt, G. Chen, and Z.F. Ren, Nano Letters **11**, 556 (2011).
[8] C. Felser, L. Wollmann, S. Chadov, G.H. Fecher, and S.S.P. Parkin, APL Mater. **3**, 041518 (2015).
[9] D.C. Ralph and M.D. Stiles, J. Magn. Magn. Mater. **320**, 1190 (2008).
[10] B. Balke, G.H. Fecher, J. Winterlik, and C. Felser, Appl. Phys. Lett. **90**, 152504 (2007).
[11] P. Kharel, Y. Huh, N. Al-Aqtash, S. Valloppilly, R.F. Sabirianov, R. Skomski, and D.J. Sellmyer, J. Phys.: Cond. Matt. **26**, 126001 (2014).
[12] J. Winterlik, S. Chadov, A. Gupta, V. Alijani, T. Gasi, K. Filsinger, B. Balke, G. H. Fecher, C.A. Jenkins, F. Casper, J. Kübler, G. D. Liu, L. Gao, S.S. P. Parkin, and C. Felser, Adv. Mat. **24**, 6283 (2012).
[13] L. Wollmann, S. Chadov, J. Kübler, and C. Felser, Phys. Rev. B **90**, 214420 (2014).
[14] H.Z. Luo, Z.Y. Zhu, G.D. Liu, S.F. Xu, G.H. Wu, H.Y. Liu, J.P. Qu, and Y.X. Li, J. Magn. Magn. Mater. **320**, 421 (2008).
[15] A. K. Nayak, M. Nicklas, S. Chadov, C. Shekhar, Y. Skourski, J. Winterlik, and C. Felser, Phys. Rev. Lett. **110**, 127204 (2013).
[16] A.K. Nayak, M. Nicklas, S. Chadov, P. Khuntia, C. Shekhar, A. Kalache, M. Baenitz, Y. Skourski, V.K. Guduru, A. Puri, U. Zeitler, J. M. D. Coey, and C. Felser, Nature Materials **14**, 679 (2015).
[17] L. Wollmann, S. Chadov, J. Kübler, and C. Felser, Phys. Rev. B **92**, 064417 (2015).